

## BRIDGELESS LANDSMAN CONVERTER AND HYSTERESIS CONTROLLER FOR POWER FACTOR CORRECTION

S.Jayaprakash

Assistant Professor, School of Electrical and Electronics, Sathyabama Institute of Science and Technology, Chennai, India. E-mail: jakash2109@gmail.com

**Abstract** – PFC is extensively used in household appliances in the form of an active front-end AC/DC converter that ensures excellent efficiency while imposing unity power factor and delivering the load with the requisite constant voltage. PFC stages have typically been used to enhance the electrical power reliability of electrical power systems by simulating an input resistance within the frequency of the system. Moreover, the input current is sinusoidal when the load voltage is sinusoidal and possess increased harmonic distortion integrated with ripples during switching process. Henceforth, in this approach, an efficient bridgeless landsman converter is exploited that facilitates the flow of current across minimal semiconductor components thereby reducing losses and improving efficiency. Without changing the carrier frequency, an LC filter is used to lessen the switching ripple amplitude, maintain a sinusoidal voltage, and reduce acoustic noise. A PI controller is utilized to attain the integral component, and the controller's output is proportional to the measurement variation or error. The hysteresis controller calculates the steady-state switching frequency of the converter along with PWM generator which minimizes the current stress. The simulation is performed in MATLAB/SIMULINK and the obtained outputs indicated minimized THD with improved efficiency.

**Keywords:** LC filter, Bridgeless landsman converter, Hysteresis controller, PI controller, PWM.

### 1 INTRODUCTION

Researchers and engineers have been working hard in recent years for improving power factor correction (PFC) as well as ensuring the absorbed current meets the requirements of standard regulations [1]. For the transfer of real power to a DC load from the AC grid, an increased power factor (PF) is essential. While power factor has previously been seen to be relevant only at power levels that are high, it is becoming increasingly essential at minimized levels of power, as evidenced by targets for applications like laptop chargers and LED drivers [2, 3]. Hence various converters are deployed for PFC and these converters are power converting stages that utilize submissive currents with designing and regulating currents at harmonic frequencies of the grid voltage associated with international standards. However, in multistage systems, stages for PFC generally comprise a large portion of the volume of overall power converter and put severe requirements on ensuing stages. As a result, improvements in PFC stages exhibit a variety of effects [4].

The traditional boost PFC converter has a greater efficiency, improved power factor (PF), enhanced density as well as minimal cost. Despite this, the ripple current of the boost capacitor is extremely more. With the rise in power level, the input rectifier losses of the system reduce the efficiency dramatically, necessitating further steps for dealing with the dissipation of heat. Furthermore, the boost converter switch is operated under difficult switching conditions, resulting in large switching losses and limiting the system's switching

frequency range. Finally, boost diode reverse recovery generates a lot of electromagnetic interference (EMI), that causes unanticipated shoot across states that harm the system and force the system to stop unexpectedly [5-9]. In contrast to the boost converter, the dual boost/bridgeless boost converter topology lacks a diode bridge rectifier. This topology decreases the total number of semiconductors in the input rectifier bridge from six to four, reducing conduction losses and the related heat management concern. Due to the PWM switches' hard-switching function, the dual boost converter has large switching losses [10]. Buck-boost converters with a broad range of input as well as output voltage have been introduced to address this issue. It converts voltage in both step-down and step-up modes, however the converter's performance is limited by the fact that its input current is discontinuous [11]. Functional variations of bridgeless PFC topologies depending on Cuk and SEPIC converters were developed to reduce conduction loss [12]. However, for the PV module's minimum voltage, its step-up static gain is insufficient. The second inductor's size of the Cuk and SEPIC converters is high, degrading the power density. Furthermore, these topologies have high quantity of passive parts, increasing cost and lowering density of power. Another problem with Cuk converters is that their output voltage is inverted, causing issues with the PV system's output connection and common ground [13-19]. Hence, a bridgeless Landsman converter is used in this technique, which paves the way for current conduction over a small number of semiconductor components, reducing losses and improving efficiency.

Using LC filters for reducing the switching ripple amplitude, results in sinusoidal voltage and minimized acoustic noise. The carrier frequency is not changed and is regarded as an efficient approach. When building an LC filter, the frequency at resonance of the voltage waveform is taken into account. To attain a virtually sinusoidal voltage, the filter's frequency at resonance is to be lower than the minimal harmonic frequency of the inverter's voltage produced by pulse width modulation (PWM) [20, 21]. A proportional integral (PI) controller is frequently employed in power converters, despite the introduction of new control approaches that use a different structure. This is due to its dependable performance under modeling situations and simple implementation [22]. Furthermore, the hysteresis controller estimates the converter's steady-state switching frequency. It functions as a frequency controller that is variable and has the merit of minimum frequency changes during variations in load [23]. PFC converters coupled in parallel and operating in the same PWM share functional power for minimizing current stress in diodes as well as major power switches. Furthermore, ripple current at the input and output capacitor size is lowered [24].

Therefore in this approach, a bridgeless landsman converter is utilized for performing efficient PFC with reduced switching losses. An LC filter is adopted to minimize the amplitude of the switching ripple thus reducing harmonics. The controlling operation is performed by the PI controller which offers easy implementation. A hysteresis controlled PWM generator is exploited to generate reliable results.

The remainder of this work is structured as: Section 2 with related concepts, section 3 includes proposed topology, section 4 with obtained results and section 5 includes conclusion.

## 2 RELATED WORKS

Amar et al [25] presented an approach which implemented 1 $\phi$  PFC utilizing boost converter in a real time manner. An increased order sliding mode controller depending on super twist algorithm was combined with controlling approaches that were predicted. In addition, the predicted approach was altered considering the wide delay of computation.

Nomar et al [26] introduced Z-source converter for the applications of PFC. The correction of power factor was performed by the network as well as the resultant system voltage was regulated during the enhancement of power factor. This improved the reliability of the system and provided boosting ability to the system.

Junwei et al [27] designed a wireless power transfer redonant converter utilizing a bridgeless boost

PFC rectifier. It improved the efficiency as well as the power quality of the line input by reducing the cost of production as well as complexity. The obtained results revealed that this approach was more enhanced when compared to conventional converters.

Toshiki et al [28] proposed a novel methodology for controlling a step-down rectifier for applying a modular converter which is multilevel in nature. The significant portion of the control system was dependent on the controlling methodology for 1 $\phi$  PFC converter. The balancing of the capacitor voltage does not demand the designing of parameters for control.

Shikha et al [29] presented a canonical switching cell which operated in DCM condition. It offered inherent PFC for broad input voltage and was connected in cascade with an isolated half bridge converter that generated multi output. The investigation of the performance was carried in conditions of steady state as well dynamic operations.

Shang et al [30] proposed a buck adopted PFC that operated in continuous conduction mode. It was manipulated by dead zone that introduced distortion in relation to the input line voltage. With the derivation of an approach for the reconstruction of predictive line voltage, the dead zone influence was mitigated. The line current of the input was shaped into sinusoidal waveform and an improved efficiency was obtained.

## 3 PROPOSED TOPOLOGY

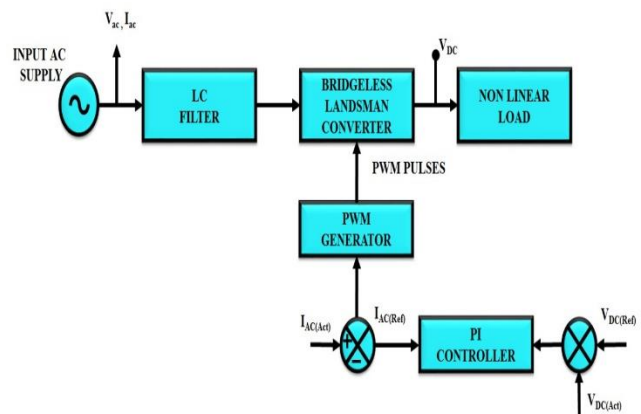


Figure 1 Proposed block diagram

The proposed block diagram is given in figure 1. The input AC supply is fed to the LC filter which is utilized for the abatement of amplitude ripples in the signal. An efficient bridgeless landsman converter is exploited in this approach for enhanced PFC with minimized switching losses. The PI controller performs the controlling operation resulting in easier implementation. A hysteresis controlled PWM generator is adopted for generating reliable results.

### 3.1 LC Filter

An LC filter is generally utilized in the input for minimizing the harmonics of input current. Generally, the LC filter is designed to possess a resonant frequency smaller than the minimized harmonic frequency. At certain cases the minimal harmonic frequency is similar to the frequency of the LC filter at resonance. The parasitic resonance of the filter is designed at a low value for reducing the losses. The LC filter prevents the overvoltages that occur in the switching operation of the converter. Figure 2 represents the AC side equivalent circuit of the LC filter.

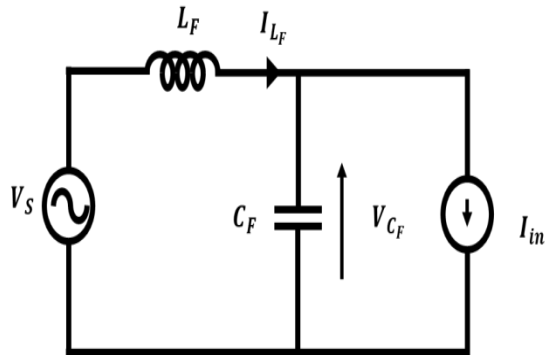


Figure 2 LC circuit

The transfer function of the LC circuit is given by,

$$\frac{I_s(S)}{I_{in}(S)} = \frac{1}{1+s^2L_fC_f} \quad (1)$$

$$\frac{V_{cf}(S)}{I_{in}(S)} = \frac{-sL_f}{1+s^2L_fC_f} \quad (2)$$

Where,  $I_s(S)$ : Laplace transform of source current

$V_{cf}(S)$ : Laplace transform of capacitor voltage of the filter

$I_{in}(S)$ : Laplace transform of input current of the converter

### 3.2 Bridgeless Landsman Converter

A bridgeless landsman converter is adopted for enhancing the power factor in this approach and the corresponding circuit diagram is given in figure 3. The proposed converter functions in both positive as well as negative half cycles in three different modes and the AC supply from the mains is applied to the converter. The switches are represented as  $S_A$  and  $S_B$ , the corresponding voltages are indicated by  $V_{SA}$  and  $V_{SB}$ . The inductors at input are represented as  $L_{IA}$  and  $L_{IB}$  and the corresponding current is indicated by  $I_{LIA}$  and  $I_{LIB}$ . The inductors at output are given by  $L_{OA}$  and  $L_{OB}$  and the corresponding current is given by  $I_{LOA}$  and  $I_{LOB}$ .

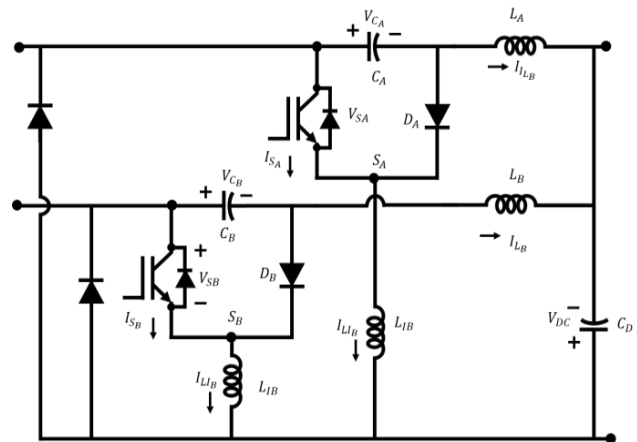


Figure 3 Bridgeless landsman converter

#### 3.2.1 Mode 1

In mode 1 as given in figure 4, when switch  $S_A$  is in ON condition, the energy supplied as well as the energy stored in intermediate capacitor  $C_A$  is transmitted to the input inductor  $L_{IA}$ . Discharging of  $L_{OA}$  occurs and voltage  $V_{CA}$  across capacitor  $C_A$  gets minimized with the increase in  $I_{LIA}$  as well as the DC voltage  $V_{DC}$ .

#### 3.2.2 Mode 2

In mode 2 as given in figure 5, the switch is turned OFF and the intermediate capacitor  $C_A$  as well as  $L_{OA}$  charges with the supply current. The input inductor  $L_{IA}$  discharges and hence,  $V_{CA}$  increases.

#### 3.2.3 Mode 3

In this mode as in figure 6, the conduction is discontinuous due to the complete discharging of  $L_{IA}$  and hence current  $I_{LIA}$  becomes zero. An increase in resultant side inductor current  $I_{LOA}$  takes place and the value of  $V_{CA}$  is reduced.

The input voltage ( $V_s$ ) fed to the PFC based Landsman converter is indicated as,

$$V_s(t) = V_m \sin(\omega_L t) \quad (3)$$

$$= V_m \sin(2\pi f_L t) \quad (4)$$

Where,  $V_m$  : supply voltage at maximum level

$f_L, \omega_L$  : line frequency of supply voltage in Hz and rad/sec respectively

$$V_{in} = \frac{2\sqrt{2}}{\pi} V_s \quad (5)$$

The duty ratio (D) for Landsman converter is expressed as,

$$D = \frac{V_{DC}}{V_{in}+V_{DC}} = \frac{V_{DC}}{|V_m \sin(\omega t)|+V_{DC}} \quad (6)$$

The current across inductors in input  $I_{LIA}$  and  $I_{LIB}$  is discontinuous and the current across inductors in output  $I_{LOA}$  and  $I_{LOB}$  and the voltage across intermediate capacitor  $V_{CA}$  are continuous in switching cycle. The value of the output inductor relies on the permissible ripple current and is expressed as,

$$L_{OA}, L_{OB} = \left(\frac{V_S^2}{P_i}\right) \frac{D}{\Delta i_{fs}} = \frac{i}{\Delta i_{fs}} \left(\frac{V_S^2}{P_i}\right) \left(\frac{V_{DC}}{V_{in}+V_{DC}}\right) \quad (7)$$

$$= \frac{i}{\Delta i_{fs}} \left(\frac{V_{Smin}^2}{P_{max}}\right) \left(\frac{V_{DCmax}}{\sqrt{2}V_{Smin}+V_{DC}}\right) \quad (8)$$

The critical input side inductor ( $L_{IC}$ ) is given by,

$$L_{ICA}, L_{ICB} = \frac{R_{in}V_{DC}D}{2V_{in}f_s} = \left(\frac{V_S^2}{P_i}\right) \frac{V_{DC}}{2V_{in}f_s} \left(\frac{V_{DC}}{V_{in}+V_{DC}}\right) \quad (9)$$

The critical inductance value related to the maximum DC link voltage is given by,

$$L_{ICA}, L_{ICB} = \left(\frac{V_{Smin}^2}{P_{max}}\right) \frac{V_{DCmax}}{2\sqrt{2}V_{Smin}f_s} \left(\frac{V_{DCmax}}{\sqrt{2}V_{Smin}+V_{DCmax}}\right) \quad (10)$$

The input inductors ( $L_{IA}, L_{IB}$ ) are selected less than the value of critical inductance ( $L_{ICA}, L_{ICB}$ ) such that,

$$L_I \ll L_{IC}$$

The intermediate capacitance value is given by,

$$C_A, C_B = \frac{V_{DC}}{\kappa\{V_{DC}+V_{in}\}f_s(V_{DC}^2/P_i)} \left(\frac{V_{DC}}{V_{in}+V_{DC}}\right) \quad (11)$$

$$= \frac{P_i}{\kappa f_s(V_{in}+V_{DC})^2} \quad (12)$$

Where,  $\kappa$  : acceptable level of ripple voltage across intermediate capacitors.

The supply voltage at maximum value is,

$$C_1, C_2 = \frac{P_{max}}{\kappa f_s(\sqrt{2}V_{Smax}+V_{DCmax})^2} \quad (13)$$

The numerical value for the DC capacitor is given by,

$$C_D = \frac{I_{DC}}{2\omega\Delta V_{DC}} = \frac{(P_i/V_{DC})}{2\omega\Delta V_{DC}} = \frac{P_i}{2\omega\Delta V_{DC}^2} \quad (14)$$

Considering the minimal DC voltage,

$$C_D = \frac{P_{min}}{2\omega\Delta V_{DCmin}^2} \quad (15)$$

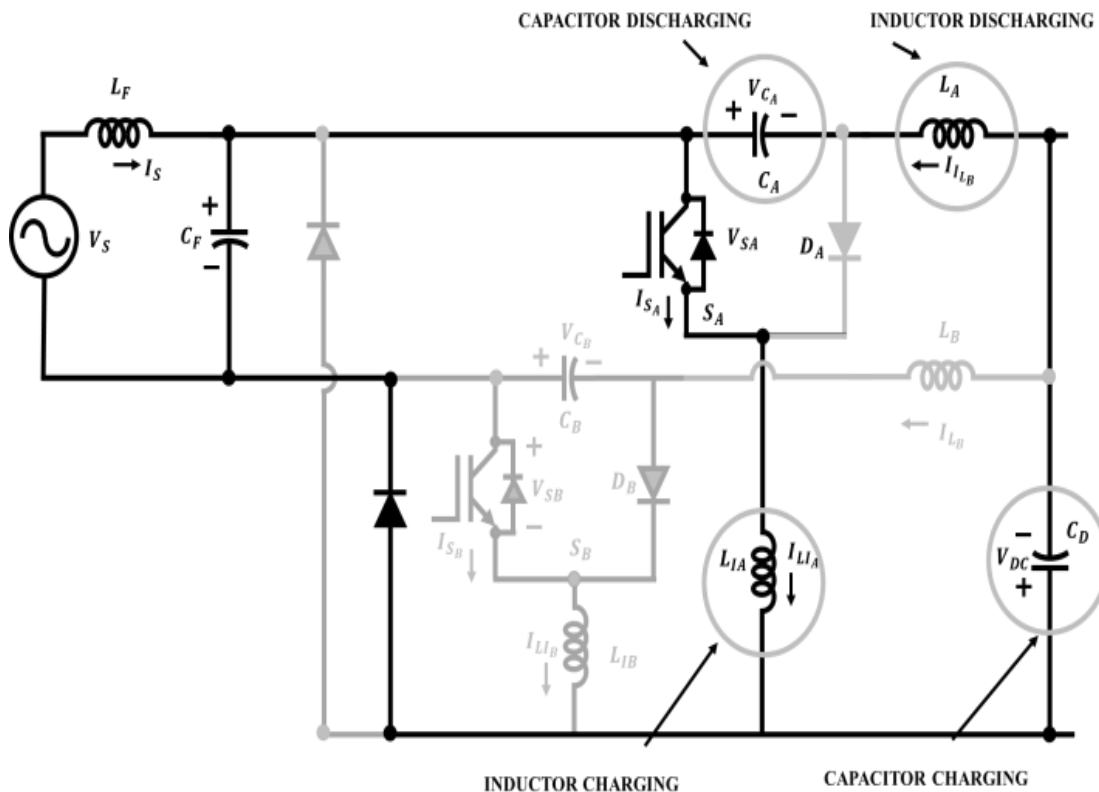


Figure 4 Operation of mode 1

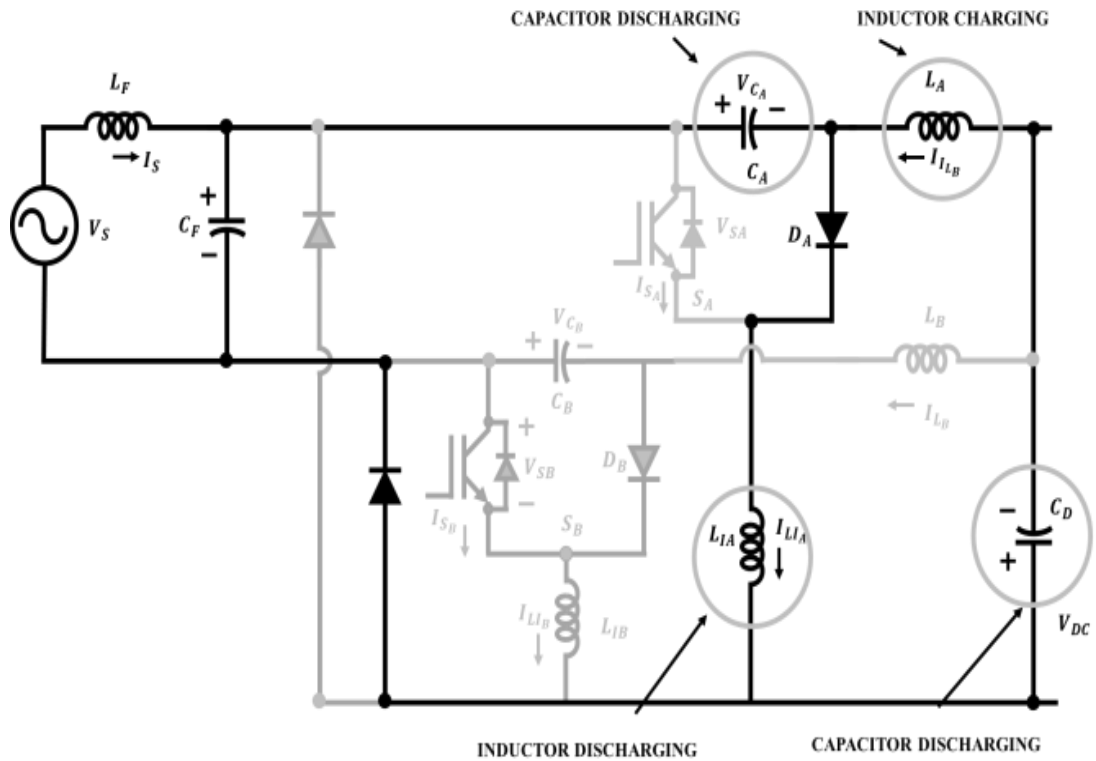


Figure 5 Operation of mode 2

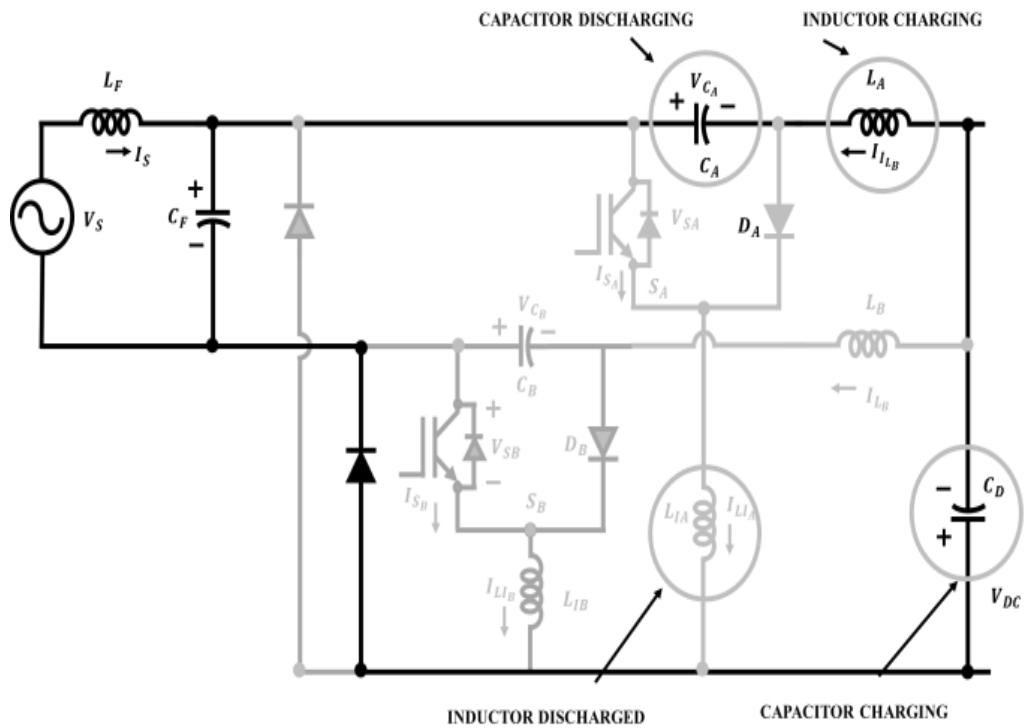


Figure 6 Operation of mode 3

### 3.3 PI Controller

A PI controller shown in figure 7 is used to obtain the integral component, and the controller's output is proportional to the measurement variation or error. Since an increase in controller gain causes loop instability, integral action is provided within the controller to eliminate this offset. The values of  $K_P$  and  $K_I$  are chosen based on the experimental step response, ensuring the system's stability. The proportional gain  $K_P$  performs the reduction of the step up time and the integral gain  $K_I$  performs the elimination of the steady state error. The controller reduces the maximum overshoot as well as improves damping. Generally, the PI controller is employed for the system control and the derivative function is sensible to the increased input frequency terms hence maintaining the stability of the system on the occurrence of noise.

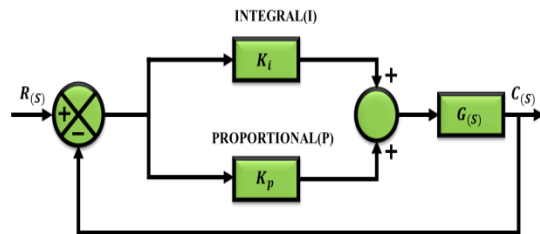


Figure 7 PI controller

### 3.4 PWM Circuit with Hysteresis Controller

Figure 8 represents a PWM circuit exploiting the hysteresis controller. The information about the inductor current is present in the feedback signal and therefore the hysteretic PWM control for the proposed converter employs ripple voltage at the output generating reliable results. This hysteresis controlled PWM circuit utilizes a hysteretic comparator and a coherent RC circuit connected across the converter's resultant terminal. A triangular voltage is effected from the RC integrated circuit and is compared with the current across the inductor depending on the comparator output. The superimposition of RC circuit's AC component with the voltage is performed at the output and is fed to the comparator input. The controller's transfer function possess derivative features and the variation of coefficient with the time constant of the RC integrated circuit occurs.  $R_A$  and  $C_A$  are connected with the resultant terminals of the comparator and a triangular voltage is obtained at the converter output. The voltage of capacitor  $C_B$  has a DC component when a square wave is obtained at the voltage of the comparator output.  $C_B$  is necessary for the coupling of AC signal with the comparator. At

switching frequency  $f_s$ , when the impedance of the capacitor is smaller than the resistance  $R_B$ , then

$$\frac{1}{2\pi f_s C_1} \ll R_2 \quad (16)$$

The voltage of capacitor  $C_A$  shows variation linearly and the voltage slope is usually estimated by  $T_C$  which is the time constant as well as the increased output level  $V_P$ . The switching frequency is expressed as,

$$f_s = \frac{DV_{CP}}{V_H T_C} \quad (17)$$

Here,  $V_H$  : hysteresis voltage

$D$  : duty cycle

$T_C$  : time constant

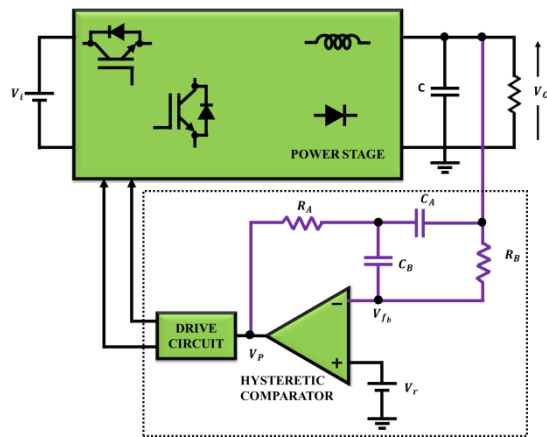


Figure 8 Hysteresis controlled PWM circuit

## 4 RESULTS AND DISCUSSION

The bridgeless landsman converter is designed and simulated in MATLAB/SIMULINK. By assessing the improvement of the power factor, the overall efficiency of the converter is determined. There occurs no phase difference between the supply voltage and current.

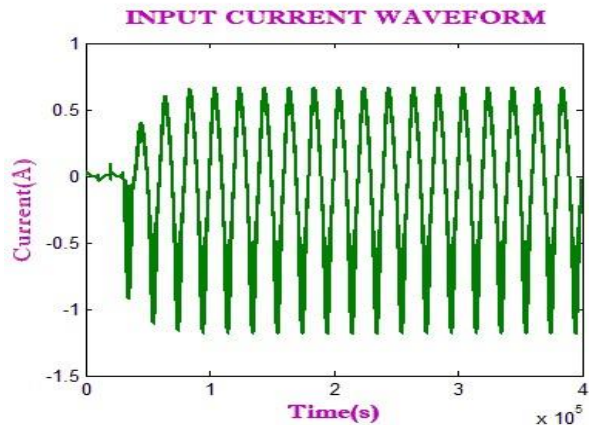


Figure 9 Waveform for input current

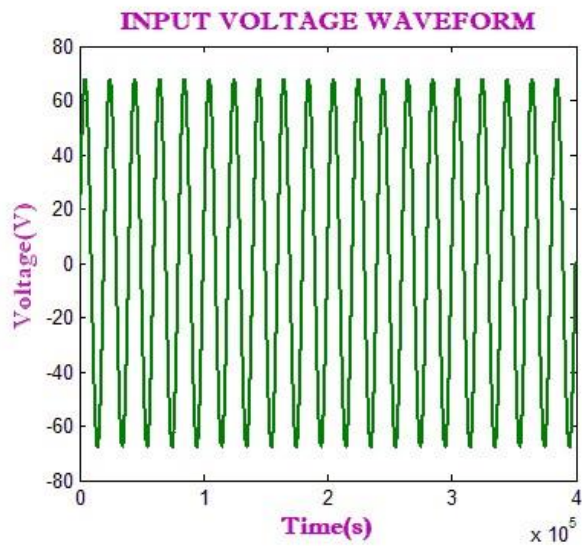


Figure 10 Waveform for input voltage

Figure 9 indicates the waveform for input current and figure 10 indicates the waveform for input voltage. These waveforms are free from harmonics due to the processing by LC filter.

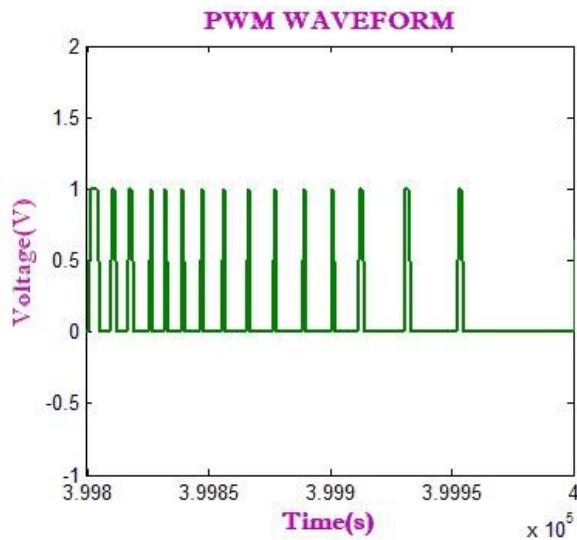


Figure 11 Waveform for PWM

Figure 11 represents the waveform for PWM generator which is generated in the form of pulses with minimized switching losses.

### CONVERTER OUTPUT CURRENT WAVEFORM

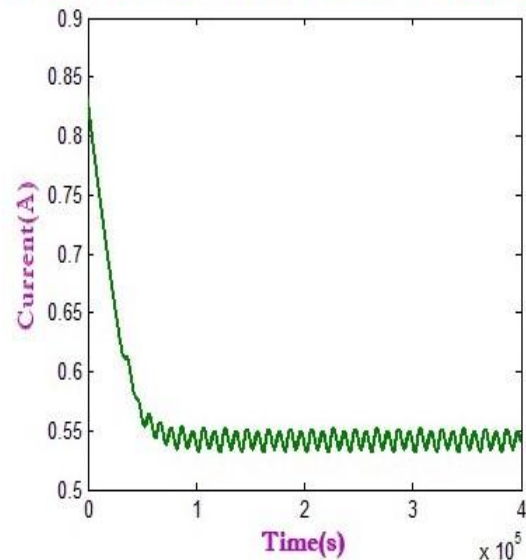


Figure 12 Waveform for converter output current

### CONVERTER OUTPUT VOLTAGE WAVEFORM

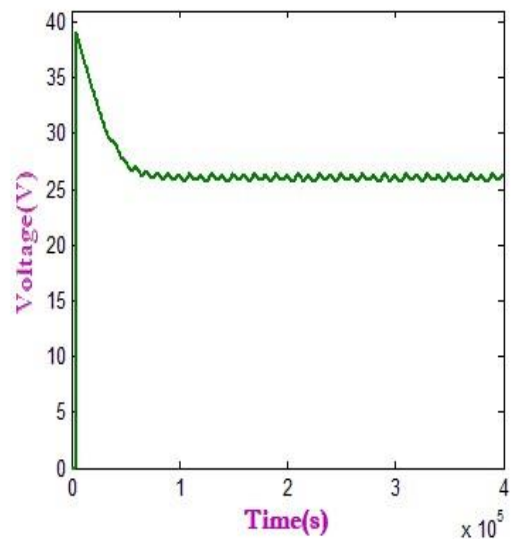
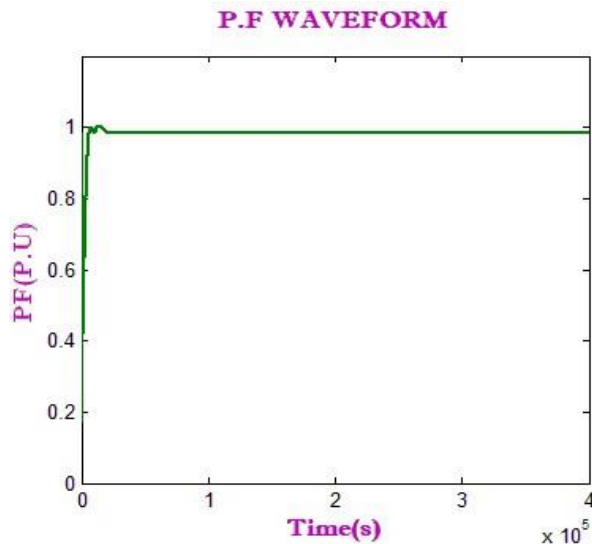


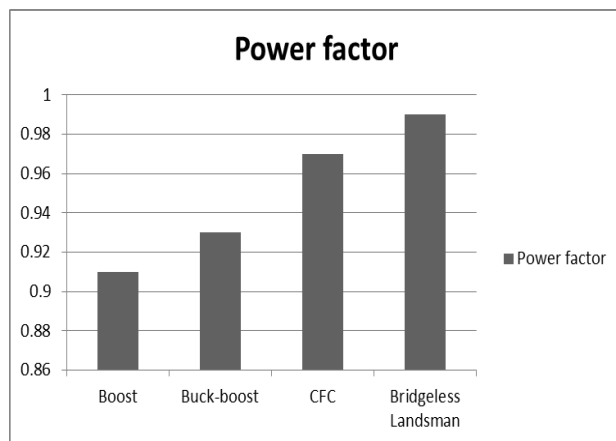
Figure 13 Waveform for converter output voltage

Figure 12 and 13 represents the output current as well as output voltage waveforms of the proposed bridgeless landsman converter respectively.



**Figure 14** Power factor waveform

Figure 14 represents the waveform for the power factor of the proposed approach. It clearly indicates that approximately a unity power factor is obtained revealing increased efficiency of the proposed approach.



**Figure 15** Comparison of power factor

Figure 15 indicates the comparison of the power factor of the proposed converter with existing converters like boost, buck-boost and CFC. From the graph it is clear that the bridgeless landsman converter showed improved power factor.

## 5 CONCLUSION

An improved PFC is obtained in this paper utilizing an efficient bridgeless landsman converter. Apart from the cost of a significant quantity of inert ingredients, this

converter was used to achieve effective control under light load situations and high efficiency. The experimental performance of the proposed approach for controlling speed over a wide variety of supply voltages has been established fairly in an effective manner. The strain of the PFC converter switch has been evaluated to ascertain its practicality and satisfactory test results have been discovered over full speed at a wide range of AC supplies. The proposed system has also been subjected to a comparative analysis in terms of efficiency and THD.

## References

- [1] Marcos-Pastor, Adria, Enric Vidal-Idiarte, Angel Cid-Pastor, and Luis Martinez-Salamero, "Interleaved digital power factor correction based on the sliding-mode approach", IEEE Transactions on Power Electronics, Vol. 31, No. 6, pp. 4641-4653, 2015.
- [2] Lim, Seungbum, David M. Otten, and David John Perreault, "New AC-DC power factor correction architecture suitable for high-frequency operation", IEEE Transactions on Power Electronics, Vol. 31, No.4, pp. 2937-2949, 2015.
- [3] Chen, Minjie, Sombuddha Chakraborty, and David J. Perreault. "Multitrack power factor correction architecture." IEEE Transactions on Power Electronics, Vol. 34, No. 3, pp.2454-2466, 2018.
- [4] Hanson, Alex J., and David J. Perreault, "A high-frequency power factor correction stage with low output voltage", IEEE Journal of Emerging and Selected Topics in Power Electronics, Vol. 8, No.3, pp.2143-2155, 2019.
- [5] Yu-Kang Lo, Chung-Yi Lin, Huang-Jen Chiu, Shih-Jen Cheng, JingYuan Lin, "Analysis and Design of a Push-Pull Quasi-Resonant Boost Power Factor Corrector in Power Electronics", IEEE Transactions on Power Electronics, Vol.28, No.1, pp.347-356, 2013.
- [6] González-Santini, Nomar S., Hulong Zeng, Yaodong Yu, and Fang Zheng Peng, "Z-source resonant converter with power factor correction for wireless power transfer applications", IEEE Transactions on Power Electronics, Vol. 31, No. 11, pp. 7691-7700, 2016.
- [7] Omar Abdel-Rahim, Haoyu Wang, "A new high gain DC-DC converter with model-predictive-control based MPPT technique for photovoltaic systems", CPSS Transactions on Power Electronics and Applications, Vol.5, No.2, pp. 191 – 200, 2020.
- [8] Balaji Chandrasekar, Chellammal Nallaperumal, Sanjeevikumar Padmanaban, Mahajan Sagar Bhaskar, Jens Bo Holm-Nielsen, Zbigniew Leonowicz, Samson O. Masebinu, "Non-Isolated High-Gain Triple Port DC-DC Buck-Boost

- Converter With Positive Output Voltage for Photovoltaic Applications”, IEEE Access, Vol. 8, pp.196500 – 196514,2020
- [9] Alam, Muntasir, Wilson Eberle, Deepak S. Gautam, Chris Botting, Nicholas Dohmeier, and Fariborz Musavi, “A hybrid resonant pulse-width modulation bridgeless AC–DC power factor correction converter”, IEEE Transactions on Industry applications, Vol. 53, No. 2, pp. 1406-1415, 2016.
- [10] Alam, Muntasir, Wilson Eberle, Deepak S. Gautam, and Chris Botting, “A soft-switching bridgeless AC–DC power factor correction converter”, IEEE Transactions on Power Electronics, Vol.32, No.10, pp.7716-7726, 2016.
- [11] Qingyun Huang, Alex Q. Huang, Ruiyang Yu;Pengkun Liu;Wensong Yu, “High-Efficiency and High-Density Single-Phase Dual-Mode Cascaded Buck–Boost Multilevel Transformerless PV Inverter With GaN AC Switches”,IEEE Transactions on Power Electronics, Vol. 34, No.8, pp. 7474 – 7488, 2019.
- [12] Anand, Aniket, and Bhim Singh, “Power factor correction in Cuk–SEPIC-based dual-output-converter-fed SRM drive”, IEEE Transactions on Industrial Electronics, Vol. 65, No. 2 , pp. 1117-1127, 2017.
- [13] Julio Cezar dos Santos de Moraes;Juliano Luiz dos Santos de Moraes;Roger Gules,“Photovoltaic AC Module Based on a Cuk Converter With a Switched-Inductor Structure”, IEEE Transactions on Industrial Electronics, Vol. 66, No.5, pp. 3881 - 3890, 2019.
- [14] Sanjeevikumar Padmanaban, Neeraj Priyadarshi, Mahajan Sagar Bhaskar, Jens Bo Holm-Nielsen, Eklas Hossain, Farooque Azam, “A Hybrid Photovoltaic-Fuel Cell for Grid Integration With Jaya-Based Maximum Power Point Tracking: Experimental Performance Evaluation”,IEEE Access, Vol. 7, pp. 82978 – 82990, 2019.
- [15] Kok Soon Tey, Saad Mekhilef;Mehdi Seyedmahmoudian, Ben Horan;Amanullah Than Oo, Alex Stojcevski, “Improved Differential Evolution-Based MPPT Algorithm Using SEPIC for PV Systems Under Partial Shading Conditions and Load Variation”, IEEE Transactions on Industrial Informatics, Vol: 14, No: 10, pp: 4322 – 4333, 2018.
- [16] Zahra Moradi-Shahrbabak;Ahmadreza Tabesh, “Effects of Front-End Converter and DC-Link of a Utility-Scale PV Energy System on Dynamic Stability of a Power System”, IEEE Transactions on Industrial Electronics, Vol.65, No. 1, pp. 403 – 411, 2018.
- [17] Kumaran Nathan,Saikat Ghosh,Yam Siwakoti,Teng Long, “A New DC–DC Converter for Photovoltaic Systems: Coupled-Inductors Combined Cuk-SEPIC Converter”, IEEE Transactions on Energy Conversion, Vol. 34, No.1, pp. 191 – 201, 2019.
- [18] Kushwaha, Radha, and Bhim Singh, “Interleaved landsman converter fed EV battery charger with power factor correction”, IEEE Transactions on Industry Applications, Vol. 56, No. 4, pp. 4179-4192, 2020.
- [19] Poorali, B., Adib, E.,”Analysis of the integrated SEPIC-flyback converter as a single-stage single-switch power-factor-correction LED driver”, IEEE Trans. Ind. Electron, Vol. 63, No. 6, pp. 3562–3569, 2016.
- [20] Yingliang Huang, Yongxiang Xu, Yong Li, Guijie Yang, Jibin Zou, “PWM Frequency Voltage Noise Cancellation in Three-Phase VSI Using the Novel SVPWM Strategy”, IEEE Transactions on Power Electronics, Vol. 33, No. 10, pp. 8596 – 8606, 2018.
- [21] Haofeng Bai, Xiongfei Wang, Frede Blaabjerg, “A Grid-Voltage-Sensorless Resistive-Active Power Filter With Series LC-Filter”, IEEE Transactions on Power Electronics, Vol. 33, No. 5, pp. 4429 – 4440, 2018.
- [22] Durgadevi, Subbiah, and Mallapu Gopinath Umamaheswari, “Analysis and design of single phase power factor correction with DC–DC SEPIC Converter for fast dynamic response using genetic algorithm optimised PI controller”, IET Circuits, Devices & Systems, Vol. 12, No. 2, pp. 164-174, 2018
- [23] Chen, Zhaoyi, Yuanrui Chen, and Zhixing Yan, “Simplified hysteresis sliding-mode control for superbuck converter”, IEEE Transactions on Circuits and Systems II: Express Briefs, Vol. 67, No.12, pp. 3212-3216, 2020.
- [24] Wang, Chien-Ming, Chang-Hua Lin, Chien-Min Lu, and Jyun-Che Li, “Design and realisation of a zero-voltage transition pulse-width modulation interleaved boost power factor correction converter”, IET Power Electronics, Vol. 8, No. 8, pp. 1542-1551, 2015.
- [25] Bouafassa, Amar, Lazhar Rahmani, and Saad Mekhilef, “Design and real time implementation of single phase boost power factor correction converter”, ISA transactions, Vol. 55, pp. 267-274, 2015.
- [26] Dian, Songyi, Xuefeng Wen, Xiang Deng, and Shimin Zhang, “Digital control of isolated Cuk power factor correction converter under wide range of load variation”, IET Power Electronics, Vol. 8, No. 1, pp. 142-150, 2015.
- [27] Liu, J., Chan, K.W., Chung, C.Y., Chan, N.H.L., Liu, M. and Xu, W, “Single-stage wireless-power-transfer resonant converter with boost bridgeless power-factor-correction rectifier”, IEEE

- Transactions on Industrial Electronics, Vol. 65, No. 3, pp.2145-2155, 2017.
- [28] Nakanishi, Toshiki, and Jun-ichi Itoh, "Control strategy for modular multilevel converter based on single-phase power factor correction converter", IEEJ Journal of Industry Applications, Vol. 6, No. pp. 46-57, 2017.
- [29] Singh, Shikha, Vashist Bist, Bhim Singh, and Gurumoorthy Bhuvaneswari, "Power factor correction in switched mode power supply for computers using canonical switching cell converter", IET Power Electronics, Vol. 8, No. 2, pp. 234-244, 2015.
- [30] Yang, Shang-Hsien, Che-Hao Meng, Chao-Chang Chiu, Chih-Wei Chang, Ke-Horng Chen, Ying-Hsi Lin, Shian-Ru Lin, and Tsung-Yen Tsai, "A buck power factor correction converter with predictive quadratic sinusoidal current modulation and line voltage reconstruction", IEEE Transactions on Industrial electronics, Vol. 63, No. 9, pp. 5912-5920, 2016.